LETTER

doi:10.1038/nature12539

Observing single quantum trajectories of a superconducting quantum bit

K. W. Murch[1,2], S. J. Weber[1], C. Macklin[1] & I. Siddiqi[1]

The length of time that a quantum system can exist in a superposition state is determined by how strongly it interacts with its environment. This interaction entangles the quantum state with the inherent fluctuations of the environment. If these fluctuations are not measured, the environment can be viewed as a source of noise, causing random evolution of the quantum system from an initially pure state into a statistical mixture—a process known as decoherence. However, by accurately measuring the environment in real time, the quantum system can be maintained in a pure state and its time evolution described by a 'quantum trajectory'[1,2] determined by the measurement outcome. Here we use weak measurements to monitor a microwave cavity containing a superconducting quantum bit (qubit), and track the individual quantum trajectories[3] of the system. In this set-up, the environment is dominated by the fluctuations of a single electromagnetic mode of the cavity. Using a near-quantum-limited parametric amplifier[4,5], we selectively measure either the phase or the amplitude of the cavity field, and thereby confine trajectories to either the equator or a meridian of the Bloch sphere. We perform quantum state tomography at discrete times along the trajectory to verify that we have faithfully tracked the state of the quantum system as it diffuses on the surface of the Bloch sphere. Our results demonstrate that decoherence can be mitigated by environmental monitoring, and validate the foundation of quantum feedback approaches based on Bayesian statistics[6–8]. Moreover, our experiments suggest a new means of implementing 'quantum steering'[9]—the harnessing of action at a distance to manipulate quantum states through measurement.

If a quantum system and its environment have a common set of stationary states, then a measurement of the environment ultimately leads to projection of the quantum system onto one of its eigenstates. Numerous experiments with photons[10], atoms[11] and solid-state systems[12,13] have elucidated this process, enabling squeezing[14–16] and quantum feedback[6–8,17]. Here we examine how real-time monitoring of a quantum system's environment reveals quantum trajectories that underlie the processes of measurement and decoherence.

In our experiment (Fig. 1a), we use a superconducting transmon circuit[18] dispersively coupled to a copper waveguide cavity in the 'three-dimensional transmon' architecture[19]. If only the two lowest levels of the transmon are considered, the qubit–cavity interaction is given by the Hamiltonian $H_{\rm int} = -\hbar\chi a^{\dagger}a\sigma_z$, where $a^{\dagger}$ and a are respectively the creation and annihilation operators for the cavity mode, σ_z is the qubit Pauli operator that acts on the qubit state in the energy basis, χ is the dispersive coupling rate and $\hbar$ is Planck's constant divided by 2π. This interaction can be viewed as either a qubit-state-dependent shift of the cavity frequency of $-\chi\sigma_z$ or a light (or a.c. Stark) shift of the qubit

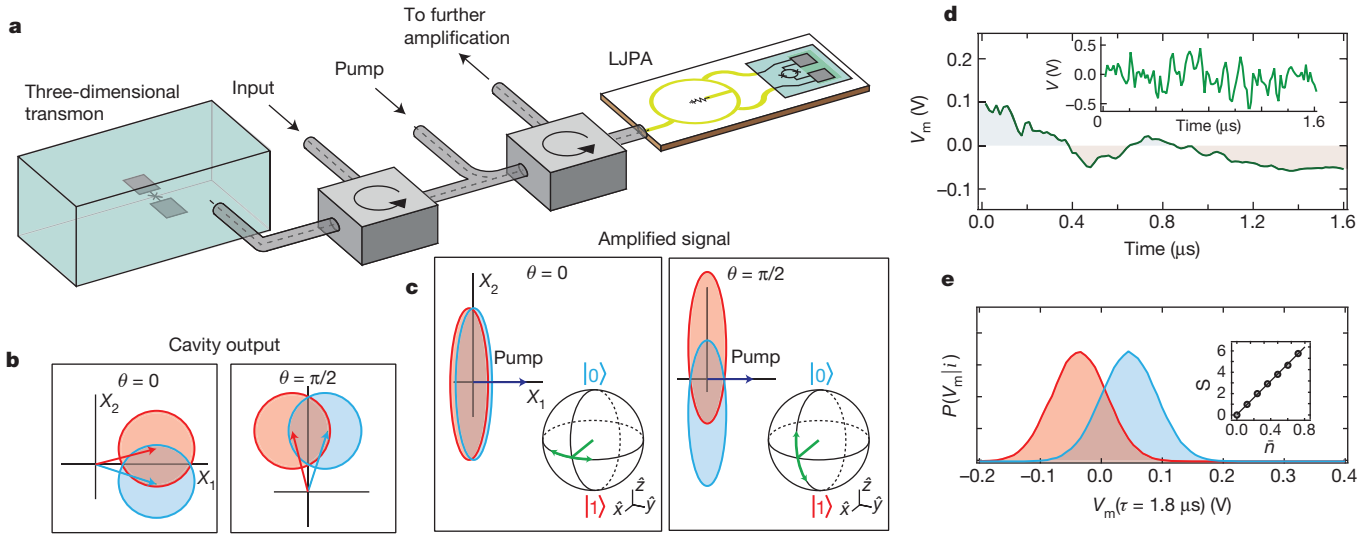

Figure 1 | Single-quadrature weak measurements. a, Our experimental set-up consists of a superconducting transmon qubit dispersively coupled to a copper waveguide cavity with a coupling rate of $\chi/2\pi = -0.49$ MHz. The cavity port sets the cavity decay rate of $\kappa/2\pi = 10.8$ MHz. Signals that reflect from the cavity are amplified by a LJPA (lumped-element Josephson parametric amplifier) operating with 10 dB of gain and an instantaneous bandwidth of 20 MHz. **b**, Illustration of the Gaussian variance of measurement signals with phases, relative to the amplifier pump, of $\theta = 0$ and $\pi/2$ after reflecting from the cavity with the qubit in $|1\rangle$ (red) or $|0\rangle$ (blue). **c**, Illustration of the measurement signal after reflecting from the LJPA. The amplifier is operated in phase-sensitive mode, where small signals that are combined in phase or in quadrature with the pump tone are respectively amplified or de-amplified, and rotated by $\pi/2$. The back-action of the measurement on a qubit superposition state is indicated on the Bloch sphere. **d**, A representative integrated measurement signal, $V_{\rm m}(\tau)$, that is obtained when the qubit is prepared in an initial superposition state along the $\hat{x}$ axis of the Bloch sphere. Inset, instantaneous measurement voltage. **e**, Histograms of $V_{\rm m}(\tau = 1.8\,\mu{\rm s})$ for the qubit prepared in $|1\rangle$ (red) and $|0\rangle$ (blue) for a measurement corresponding to $\theta = \pi/2$ with $S = 3.2$. Inset, S versus $\bar{n}$, with the solid line indicating the expected dependence for $\eta = 0.49$.

[1]Quantum Nanoelectronics Laboratory, Department of Physics, University of California, Berkeley, California 94720, USA. [2]Department of Physics, Washington University, St Louis, Missouri 63130, USA.

frequency that depends on the intracavity photon number $\hat{n}=a^{\dagger}a$. A microwave tone that probes the cavity near its resonance frequency acquires a qubit-state-dependent phase shift (Fig. 1b). For $|\chi|\ll\kappa$, where κ is the cavity decay rate, the reflected signal component in quadrature with the input measurement tone contains qubit state information, and the signal component in phase with the measurement tone carries information about the intracavity photon number. After leaving the cavity, the signal is displaced to the origin of the X_1–X_2 plane (X_1 and X_2 are the two quadrature amplitudes of the mode of the electromagnetic field) by a coherent tone and amplified by a near-quantum-limited lumped-element Josephson parametric amplifier[5] (LJPA). Phase-sensitive operation of the LJPA permits noiseless amplification of one quadrature of the reflected measurement signal with corresponding de-amplification of the other quadrature[20,21].

In principle, for an ideal amplifier, that is, one which adds no noise, the choice of measurement quadrature determines the type of back-action imparted on a coherent superposition of qubit states[22]. When the amplified quadrature conveys information about the qubit state, the measurement causes random motions of the qubit towards its eigenstates, which are located at the poles of the Bloch sphere. From the perspective of the qubit, the intracavity photon number does not fluctuate. However, when the amplified quadrature encodes the intracavity photon number, the phase of the coherent superposition evolves in response to variations in the a.c. Stark shift of the qubit and superpositions of the measurement eigenstates are not projected.

We first focus on the case in which the amplified quadrature conveys qubit state information, which we denote a 'Z-measurement'. Figure 1d displays a single measurement signal, $V_{\rm m}(\tau)=(1/\tau)\int_0^{\tau}V(t)\,{\rm d}t$, where $V(t)$ is the instantaneous measurement voltage, that is obtained when the qubit is initialized in the superposition state $(|0\rangle+|1\rangle)/\sqrt{2}$ along the $\hat{x}$ axis of the Bloch sphere. As the measurement duration increases, information about the qubit state accumulates. The best estimate for the state of the qubit after a weak measurement can be obtained using Bayes' rule[10,22,23], to find the probability of the qubit being in state i, conditioned on the integrated measurement value $V_{\rm m}$:

$$P(i|V_{\rm m})=\frac{P(i)P(V_{\rm m}|i)}{P(V_{\rm m})}$$

Probability distributions $P(V_{\rm m}|i)$ for $V_{\rm m}$ are shown in Fig. 1e for the states $i=\{|0\rangle,|1\rangle\}$. The probability $P(i)$ describes our knowledge of the prior distribution and is 1/2 when the qubit is initialized along $\hat{x}$. Thus, after acquiring a measurement value $V_{\rm m}$, the state of the system is described by[22]

$$Z^{Z}=\tanh(V_{\rm m}S/2\Delta V) \quad (1)$$

$$X^{Z}=\sqrt{1-(Z^{Z})^{2}}\,{\rm e}^{-\gamma\tau} \quad (2)$$

Here we define the expectation values of the Pauli operators conditioned on measurement value $V_{\rm m}$ as $X=\langle\sigma_x\rangle|_{V_{\rm m}}$, $Y=\langle\sigma_y\rangle|_{V_{\rm m}}$ and $Z=\langle\sigma_z\rangle|_{V_{\rm m}}$, where the superscript 'z' denotes a Z-measurement and $S=64\tau\chi^2\bar{n}\eta/\kappa$ is the dimensionless measurement strength that depends on the measurement duration, τ, the quantum efficiency of the measurement, η, and the average intracavity photon number, $\bar{n}$. The measurement strength can also be related to the separation between the measurement probability distributions for the states $|0\rangle$ and $|1\rangle$, ΔV, and their Gaussian variance, σ^2: $S=(\Delta V)^2/\sigma^2$. We calibrate $\bar{n}$ using the measured a.c. Stark shift of the qubit frequency. From a linear fit of S to $\bar{n}$ (Fig. 1e, inset), we determine that $\eta=0.49$. For small values of S, an individual measurement does not fully determine the qubit state. For $S\gg1$, the histograms are well separated and the qubit state can be determined with very high confidence, corresponding to a projective measurement.

The exponential decay of coherence in X^Z in equation (2) reflects imperfect knowledge about the state of the environment and leads to qubit dephasing characterized by the rate $\gamma=8\chi^2\bar{n}(1-\eta)/\kappa+1/T_2^*$. The first term here reflects measurement-induced dephasing[24,25] originating from the degree to which the signal is undetected (quantified by $1-\eta$). The second term reflects extra environmental dephasing, which is characterized by $T_2^*=20\ \mu$s for the qubit.

We now discuss the case of a 'ϕ-measurement', in which the amplified quadrature encodes the fluctuating intracavity photon number. Each photon that enters the cavity shifts the qubit phase by an average of $4\chi/\kappa$, causing the phase of a coherent superposition of the qubit states $|0\rangle$ and $|1\rangle$ to evolve. Given ΔV and S (obtained from a separate Z-measurement), $V_{\rm m}$ can be used to infer the total accrued phase shift. The evolution of X and Y is then given by[22]

$$X^{\phi}=\cos(SV_{\rm m}/2\Delta V){\rm e}^{-\gamma\tau} \quad (3)$$

$$Y^{\phi}=-\sin(SV_{\rm m}/2\Delta V){\rm e}^{-\gamma\tau} \quad (4)$$

The back-action associated with quadrature specific amplification, as given by equations (1)–(4), is presented in Fig. 2. To verify these predictions, we conduct an experiment consisting of three primary actions: we first prepare the qubit along the $\hat{x}$ axis, then we digitize the amplified measurement tone for 1.8 μs and, finally, we measure the projection of the qubit state along the $\hat{x}$, $\hat{y}$ or $\hat{z}$ axis. After repeating the experiment sequence $\sim10^5$ times, we evaluate X^Z, X^{ϕ}, Y^Z, Y^{ϕ}, Z^Z and Z^{ϕ}. Figure 2c displays the results of this measurement procedure for a Z-measurement, as a function of $V_{\rm m}$. A measurement with $V_{\rm m}=0$ yields no information about the qubit state, leaving it unperturbed. A strongly positive or negative value of $V_{\rm m}$, although rare, corresponds to a significant motion of the qubit towards the state $|0\rangle$ or, respectively, the state $|1\rangle$. For the ϕ-measurement (Fig. 2d), Z^{ϕ} is uncorrelated with the measurement signal. Here $V_{\rm m}$ conveys information about the phase shift of the qubit state resulting from the fluctuating intracavity photon number.

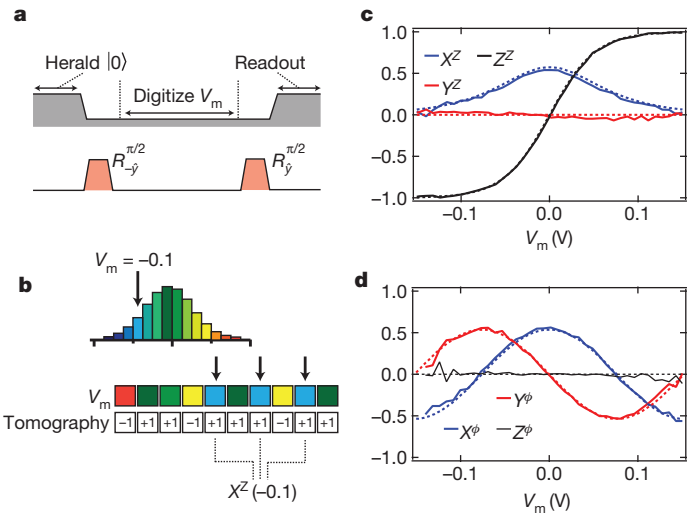

Figure 2 | Correlation of tomography results with measurement values. **a**, Experimental sequence for determining X^Z. An initial strong measurement is used to herald $|0\rangle$, and this is followed by a rotation about the $\hat{y}$ axis to prepare the qubit along $\hat{x}$. A weaker measurement signal is digitized for 1.8 μs, and a final rotation and strong measurement are used to determine the qubit projection along $\hat{x}$. Similar sequences are used to determine Y^Z and Z^Z. **b**, Tomography correlation procedure. Different measurement values are indicated as different colours, with the colour-coded histogram indicating the relative probability of each measurement value. Boxes indicate the measurement value, $V_{\rm m}$, for each experimental repetition, and the associated tomography result is indicated as ±1. Tomography results for matching $V_{\rm m}$ are averaged together to determine X^Z. **c**, Tomography results versus $V_{\rm m}$ for a Z-measurement with $\bar{n}=0.4$. The dashed lines are theory curves based on equations (1) and (2) for $\eta=0.49$ and $S=3.15$, where $\gamma=2.8\times10^5\ {\rm s}^{-1}$. **d**, Tomography results for a ϕ-measurement for $\bar{n}=0.46$. The dashed lines are theory curves based on equations (3) and (4) for $\eta=0.49$ and S = 3.62, where $\gamma=3.1\times10^5\ {\rm s}^{-1}$.

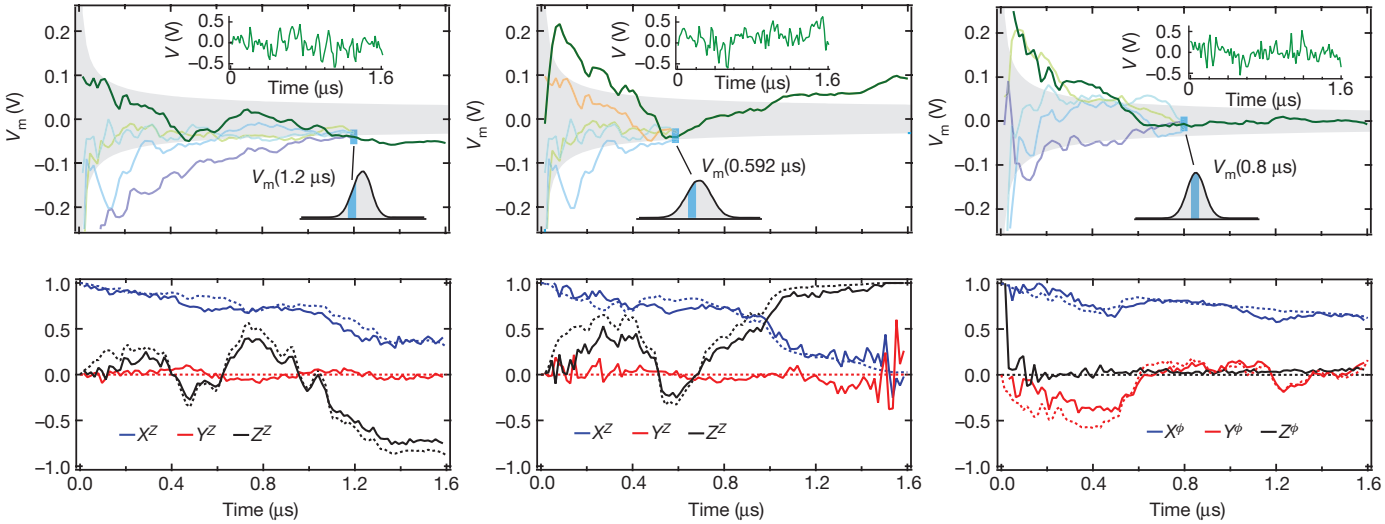

Figure 3 | Quantum trajectories. **a**, **b**, Individual measurement traces obtained for Z-measurements with $\bar{n} = 0.4$. The top panels display $V_m(\tau)$ as a green line, with the upper insets displaying the instantaneous measurement voltage. The grey region indicates the standard deviation of the distribution of measurement values. Measurement traces that converge to an integrated value within the blue matching window are used to reconstruct, using tomography, the trajectory at that time point. A few different measurement traces that contribute to the reconstruction at 1.2 μs (**a**) and 0.592 μs (**b**) are indicated in lighter colours. The lower insets indicate the distribution of measurement values with the blue matching window. The lower panels display quantum trajectories obtained from analysis of the measurement signal, as dotted lines. Solid lines indicate the tomographically reconstructed quantum trajectory based on the ensemble of measurements that are within the matching window of the original measurement signal. **c**, Individual measurement traces and associated quantum trajectories obtained for a ϕ-measurement with $\bar{n} = 0.4$.

For both types of measurement, the results show excellent agreement with theory for $\eta = 0.49$.

We have so far demonstrated that the integrated measurement signal provides a faithful record of the fluctuations of the environment and the associated motions of the qubit state. Moreover, we observe that the direction of motion of the qubit state depends on the amplification quadrature. To examine quantum trajectories of the system, we divide the measurement signal into successive segments. The integrated measurement signal can then be written as a string $\{V_m(\tau_0), V_m(\tau_1), V_m(\tau_2), \ldots\}$, where $\tau_{i+1} - \tau_i = 16$ ns. At each time point, $V_m(\tau_i)$ can be used to infer the qubit state. In Fig. 3, we present measurement traces along with the quantum trajectory of the system associated with each noisy measurement trace. The trajectories show how the quantum system evolves stochastically from an initial state prepared along $\hat{x}$ towards a final state. Measurement inefficiency and additional dephasing limits the accuracy with which the state can be tracked. This limitation is manifest as a gradual shortening of the estimated transverse coherence of the qubit state.

To verify that we have accurately inferred the quantum trajectory of the system corresponding to a given measurement signal, we perform quantum state tomography on an ensemble of experimental iterations with similar measurement values. A tomographic reconstruction of the trajectory is obtained by making measurements of variable duration, τ_i, and subsequently measuring the projection of the qubit state along one of the Cartesian axes of the Bloch sphere. Only measurements with values that are within $\pm\varepsilon$ of the target value, $V_m(\tau_i)$, contribute to determining the ensemble properties X, Y and Z. As shown in the upper panels of Fig. 3, many different measurement signals that converge to $V_m(\tau_i) \pm \varepsilon$ at τ_i are used in the tomographic reconstruction. This illustrates how the inferred state at a particular time depends only on the value of the integrated measurement voltage at that time.

Figure 3a, b displays quantum trajectories that are obtained for Z-measurements. The reconstructed trajectories based on ensemble measurements, shown as solid lines, are in reasonable agreement with the quantum trajectories determined from a single measurement record, and reproduce many of the minute motions of the qubit as it ultimately evolves towards its eigenstates of measurement. Some trajectories highlight the concept of quantum measurement reversal:[26–29] in Fig. 3a, after ~400, 600 and 1,000 ns of measurement the qubit state has returned nearly to its original state, effectively 'reversing' the preceding partial collapse of the qubit wavefunction. In Fig. 3c, we display the measurement record that we obtain from a ϕ-measurement. The resulting quantum trajectory is confined to motions along the equator of the Bloch sphere.

Full control over the environment of a quantum system allows for the mitigation of decoherence through accurate monitoring of fluctuations of the environment. Although measurement schemes based on projective measurements on ancilla qubits obtain measurement efficiencies[30] greater than 0.9, the measurement efficiency presented here, $\eta = 0.49$, is among the highest reported values for a continuous variable[6–8,13]. This efficiency is limited by an imperfect collection efficiency, $\eta_{col} = 0.72$, resulting from losses in microwave components, and imperfect amplifier quantum efficiency, $\eta_{amp} = 0.68$. Further improvements in the quantum measurement efficiency will be essential for realizing potential applications of quantum feedback[6,7] in quantum metrology and information science.

METHODS SUMMARY

The qubit consists of two aluminium paddles connected by a double-angle-evaporated aluminium superconducting quantum interference device (SQUID) deposited on double-side-polished silicon, and is characterized by charging and Josephson energies $E_c/h = 200$ MHz and $E_J/h = 11$ GHz, respectively. The qubit is operated with negligible flux threading the SQUID loop with transition frequency $\omega_q/2\pi = 3.999$ GHz. The qubit is located off centre of a 6.8316-GHz copper waveguide cavity.

The LJPA consists of a two-junction SQUID, formed from 2-μA Josephson junctions, shunted by 3 pF of capacitance, and is flux-biased to provide 10 dB of gain at the cavity resonance frequency. The LJPA is pumped by two sidebands that are equally spaced 300 MHz above and below the cavity resonance. A second LJPA that follows the first provides additional gain. A detailed experimental schematic is shown in Supplementary Fig. 1.

Experiment sequences start with an 800-ns readout with $S = 42$ that is used to herald the state $|0\rangle$ at the beginning of the experiment. A sample herald histogram is shown in Supplementary Fig. 2. Because $|\chi| \ll \kappa$, several peaks are visible, corresponding to the many energy levels of the transmon qubit. After preparing the state $|0\rangle$, we perform a 16-ns $\pi/2$-rotation about the $-\hat{y}$ axis to initialize the qubit along the $\hat{x}$ axis. After a period of variable duration, we perform quantum state tomography, which consists of either rotations about the $\hat{x}$ and $\hat{y}$ axes or no rotation and a second 800-ns readout with $S = 42$. In a fraction (~4%) of the final readouts, the qubit is outside the $\{|0\rangle, |1\rangle\}$ manifold. These sequences were disregarded in the analysis. Tomography results are corrected for the readout fidelity of 95%.

Received 29 May; accepted 7 August 2013.

1. Carmichael, H. *An Open Systems Approach to Quantum Optics* (Springer, 1993).
2. Carmichael, H. J., Kochan, P. & Tian, L. In *Proc. Int. Symp. Coherent States: Past, Present, and Future* (eds Feng, D. H., Strayer, M. R. & Klauder, J. R.) 75–91 (World Scientific, 1994).
3. Gambetta, J. *et al.* Quantum trajectory approach to circuit QED: quantum jumps and the Zeno effect. *Phys. Rev. A* **77,** 012112 (2008).
4. Castellanos-Beltran, M. A., Irwin, K. D., Hilton, G. C., Vale, L. R. & Lehnert, K. W. Amplification and squeezing of quantum noise with a tunable Josephson metamaterial. *Nature Phys.* **4,** 929–931 (2008).
5. Hatridge, M., Vijay, R., Slichter, D. H., Clarke, J. & Siddiqi, I. Dispersive magnetometry with a quantum limited squid parametric amplifier. *Phys. Rev. B* **83,** 134501 (2011).
6. Sayrin, C. *et al.* Real-time quantum feedback prepares and stabilizes photon number states. *Nature* **477,** 73–77 (2011).
7. Vijay, R. *et al.* Stabilizing Rabi oscillations in a superconducting qubit using quantum feedback. *Nature* **490,** 77–80 (2012).
8. Campagne-Ibarcq, P. *et al.* Persistent control of a superconducting qubit by stroboscopic measurement feedback. *Phys. Rev. X* **3,** 021008 (2013).
9. Schrödinger, E. Die gegenwärtige Situation in der Quantenmechanik. *Naturwissenschaften* **23,** 807–812,–823–824, 844–849 (1935).
10. Guerlin, C. *et al.* Progressive field-state collapse and quantum non-demolition photon counting. *Nature* **448,** 889–893 (2007).
11. Kuzmich, A. *et al.* Quantum nondemolition measurements of collective atomic spin. *Phys. Rev. A* **60,** 2346–2350 (1999).
12. Vijay, R., Slichter, D. H. & Siddiqi, I. Observation of quantum jumps in a superconducting artificial atom. *Phys. Rev. Lett.* **106,** 110502 (2011).
13. Hatridge, M. *et al.* Quantum back-action of an individual variable-strength measurement. *Science* **339,** 178–181 (2013).
14. Kuzmich, A., Mandel, L. & Bigelow, N. P. Generation of spin squeezing via continuous quantum nondemolition measurement. *Phys. Rev. Lett.* **85,** 1594–1597 (2000).
15. Takano, T., Fuyama, M., Namiki, R. & Takahashi, Y. Spin squeezing of a cold atomic ensemble with the nuclear spin of one-half. *Phys. Rev. Lett.* **102,** 033601 (2009).
16. Schleier-Smith, M. H., Leroux, I. D. & Vuletić, V. States of an ensemble of two-level atoms with reduced quantum uncertainty. *Phys. Rev. Lett.* **104,** 073604 (2010).
17. Ristè, D., Bultink, C. C., Lehnert, K. W. & DiCarlo, L. Feedback control of a solid-state qubit using high-fidelity projective measurement. *Phys. Rev. Lett.* **109,** 240502 (2012).
18. Koch, J. *et al.* Charge-insensitive qubit design derived from the Cooper pair box. *Phys. Rev. A* **76,** 042319 (2007).
19. Paik, H. *et al.* Observation of high coherence in Josephson junction qubits measured in a three-dimensional circuit QED architecture. *Phys. Rev. Lett.* **107,** 240501 (2011).
20. Caves, C. M. Quantum limits on noise in linear amplifiers. *Phys. Rev. D* **26,** 1817–1839 (1982).
21. Clerk, A. A., Devoret, M. H., Girvin, S. M., Marquardt, F. & Schoelkopf, R. J. Introduction to quantum noise, measurement, and amplification. *Rev. Mod. Phys.* **82,** 1155–1208 (2010).
22. Korotkov, A. N. Quantum Bayesian approach to circuit QED measurement. Preprint at http://arxiv.org/abs/1111.4016 (2011).
23. Wiseman, H. & Milburn, G. *Quantum Measurement and Control* (Cambridge Univ. Press, 2010).
24. Schuster, D. I. *et al.* ac Stark shift and dephasing of a superconducting qubit strongly coupled to a cavity field. *Phys. Rev. Lett.* **94,** 123602 (2005).
25. Boissonneault, M., Gambetta, J. M. & Blais, A. Dispersive regime of circuit QED: photon-dependent qubit dephasing and relaxation rates. *Phys. Rev. A* **79,** 013819 (2009).
26. Korotkov, A. N. & Jordan, A. N. Undoing a weak quantum measurement of a solid-state qubit. *Phys. Rev. Lett.* **97,** 166805 (2006).
27. Katz, N. *et al.* Coherent state evolution in a superconducting qubit from partial-collapse measurement. *Science* **312,** 1498–1500 (2006).
28. Katz, N. *et al.* Reversal of the weak measurement of a quantum state in a superconducting phase qubit. *Phys. Rev. Lett.* **101,** 200401 (2008).
29. Kim, Y.-S., Lee, J.-C., Kwon, O. & Kim, Y.-H. Protecting entanglement from decoherence using weak measurement and quantum measurement reversal. *Nature Phys.* **8,** 117–120 (2012).
30. Groen, J. P. *et al.* Partial-measurement back-action and non-classical weak values in a superconducting circuit. *Phys. Rev. Lett.* **111,** 090506 (2013).

Supplementary Information is available in the online version of the paper.

Acknowledgements We thank H. Wiseman, A. N. Korotkov, E. M. Levenson-Falk and N. Roch for discussions, and R. Vijay for contributions to preliminary experiments. This research was supported in part by the Army Research Office, Office of Naval Research and the Office of the Director of National Intelligence (ODNI), Intelligence Advanced Research Projects Activity (IARPA), through the Army Research Office. All statements of fact, opinion or conclusions contained herein are those of the authors and should not be construed as representing the official views or policies of IARPA, the ODNI or the US government.

Author Contributions K.W.M. and S.J.W. performed the experiment, analysed the data and wrote the manuscript. C.M. had the idea for the experiment and edited the manuscript. All work was carried out under the supervision of I.S.

Author Information Reprints and permissions information is available at www.nature.com/reprints. The authors declare no competing financial interests. Readers are welcome to comment on the online version of the paper. Correspondence and requests for materials should be addressed to K.W.M. (katerm@berkeley.edu).